Materials Advances

Accepted Manuscript

This article can be cited before page numbers have been issued, to do this please use: S. Venkatesan, J. Sivanadanam, K. Ramanujam and M. Asha Jhonsi, *Mater. Adv.*, 2020, DOI: 10.1039/D0MA00654H.

ROYAL SOCIETY OF CHEMISTRY

rsc.li/materials-advances

View Article Online
DOI: 10.1039/D0MA00654H

ARTICLE

Delineating the Enhanced Efficiency of Carbon Nanomaterials Included Hierarchical Architecture of Photoanode of Dye Sensitized Solar Cells

Received 00th January 20xx,
Accepted 00th January 20xx

DOI: 10.1039/x0xx00000x

Venkatesan Srinivasan[a], Jagadeeswari Sivanadanam[b*], Kothandaraman Ramanujam[b], Mariadoss Asha Jhonsi[a*]

Dye sensitized solar cells are economical and easy to fabricate in comparison to the silicon-based solar cells. Visible light sensitizer dye is the heart of the DSSCs, whose performance can be enhanced if the engineering of the TiO_2 semiconductor is adopted to maximize the utilization of the dye along with easy regeneration of dye from its oxidized form. In this study, a hierarchical porous architecture was imparted to the TiO_2 photoanode using size selected (1.5 to 3 nm) carbon nanomaterials (CNMs). This porous structure enhanced the accessibility of the dyes to the electrolyte. Using N719 dye as a model system, the effect of the hierarchical porous structure was demonstrated. The inclusion of CNMs, along with TiO_2, has enhanced the short circuit current density by 31 % and power conversion efficiency (PCE) by 46% compared to CNMs free DSSCs.

Introduction

There is a continuous surge in energy demand due to the energy-intensive activity of human beings. As a result, the non-replenishable sources are insufficient for our future expansion of energy economy, and this motivated the researchers to explore the environmentally benign renewable energy sources. Therefore, harnessing the inexhaustible and clean source, solar energy, via photovoltaic occupies the central stage of renewable energy research.[1] In the past two decades, a significant advancement in the photovoltaic arena and efficiencies as high as 40% was achieved by multijunction solar cell technologies. Among the various photovoltaic options, dye sensitized solar cells (DSSCs) considered being cheaper due to its ease of fabrication and involvement of ubiquitously available materials in their making.

In DSSC, besides dye, wide bandgap semiconductors such as TiO_2 and ZnO play a pivotal role in light harvesting. TiO_2 offers a conducting pathway for transporting electron from the excited state (lowest unoccupied molecular orbital (LUMO)) of dye to the conductive back contact via its conduction band (CB) and anchors sufficient dye/photosensitizers via its high surface area. In light of the previous statement, energy level matching of the dye-semiconductor interface, and rationally designed semiconductor film (to reduce the loss of illuminating light, loss of injected electrons by recombination with holes, defects and crystal boundaries) are essential. A straightforward way to significantly up the performance of DSSCs is by manipulating semiconductor film with its morphology and crystal phase. In the past, photoanodes were improvised using nano-architectures,[3-5] light scattering layer,[6,7]composite with another semiconductor[8-10] or graphene,[11,12] doping,[13-15] interfacial engineering[16,17] and $TiCl_4$ post-treatment methods.[18,19] For instance, various nanoforms of ZnO was used as cascading co-sensitized nanomaterial which enhanced the efficiency of dye sensitized solar cells[20,21] and Vanadium doped TiO_2 is used to fabricate the working electrode in a DSSCs by layer-by-layer method was explored a remarkable performance compared to bare TiO_2 particles[22].

Electron transfer within TiO_2 particles occurs by two phenomena: percolation through the network of particles and thermal accessibility to high energy states. To improve the electron transport, TiO_2 was explored in various nanostructures like nanotubes,[23] nanowires,[24] hierarchical structures,[25] and specifically exposed facets,[26]etc. A film made of ~20 nm sized TiO_2 nanoparticles generally makes the semiconductor layer meet energy level matching and to host a sufficient amount of dyes. In this architecture, the electron adopts a random walk process encountering many grain boundaries, trap states, and defects, which results in huge electron recombination if the interface is not well engineered. One way to achieve improved PCE is to use hierarchical spheres of TiO_2 to make a secondary structure which is concentric spherical or three dimensional in shape.[27] These materials are known for their high light-harvesting and lower electron recombination,[28,29] as they promote light scattering and electron transport.

[a]Department of Chemistry, B. S. Abdur Rahman Crescent Institute of Science and Technology, Vandalur, Chennai – 600 048, Tamil Nadu, India.
[b]Department of Chemistry, Indian Institute of Technology Madras, Chennai –36, Tamil Nadu, India.
E-mail: jhonsiasha@gmail.com (Mariadoss Asha Jhonsi);
Jagadhi333@gmail.com (Sivanadanam Jagadeeswari)
(All the authors have equally contributed to this work, Dr. KR facilitated writing the manuscript)

Electronic Supplementary Information (ESI) available: [Characterization of nanomaterial and other spectral data]. See DOI: 10.1039/x0xx00000x

Novel materials such as plasmonic metal nanoparticles (gold and silver nanoparticles),[30] photonic crystals,[31] WO_3-thiol coated Au, and nanocarbon/carbon-based nanomaterials[32] were incorporated to improvise the DSSC. Among the various materials composited with TiO_2 in a DSSC device, carbon-based nanomaterials[33] are interesting owing to their synergistic and intrinsic properties. Carbon-based nanomaterials are generally manufactured via both top-down (electrodeposition, laser ablation, exfoliation form graphite etc.) and bottom-up approaches (solvo/hydrothermal, microwave assisted, ultrasonic synthesis etc.).[34,35] It is reported the addition of some wt% of carbon nano in TiO_2 which could perk up the efficiency of a DSSC device. For instance, Yu et al. improvised PCE upto 25% by incorporating 0.75 wt.% of graphene with TiO_2 nanosheet. Carbon nanotubes were also explored for its ability to reduce the charge recombination. By and large, graphene is preferred over 1D carbon nanotubes as later has fewer intermolecular forces and connections (point contact) with TiO_2. Graphene exhibit an electron mobility of 15000 $cm^2\ V^{-1}s^{-1}$, which explored better performance compared to ZnO (200 – 1000 $cm^2\ V^{-1}s^{-1}$) and TiO_2 (0.1 – 4 $cm^2\ V^{-1}s^{-1}$). Often, the amount of carbon nanomaterials reported is less than 1 wt.% as loadings over that generally shield the visible light from being harvested by the dyes affecting the population of photogenerated electrons and PCE. Xiang et al. have incorporated 0.2 wt.% of nitrogen-reduced graphene oxide, which enhanced the PCE to 7.19% from 6.42 % by circumventing the electron recombination and the increasing the electron transfer efficiency.[36] To alleviate limitations associated with 1D nanomaterial, a 2D graphene (zero bandgap material) was explored as a bridge in nanocrystalline semiconductor photoanode, due to its lower transfer barrier bestowing lower recombination rate. Besides, the light scattering effect of 2D graphene improved the short-circuit current density (*Jsc*) by 45% and PCE by 39% without sacrificing the open circuit voltage (*Voc*).[37] A DSSC with anatase TiO_2 @1.6wt.% reduced graphene oxide composite material prepared by two steps hydrothermal method and stained by N719 dye showed a PCE of 7.68%, which is higher than the pristine anatase (4.78%).[38] Chen et al. demonstrated the effect of graphene content in device performance; they have attained an overall PCE of 7.1% of PCE at an optimum graphene content of 2 wt.%, beyond which light harvesting was affected negatively.[39]

Based on the reported literature, it is observed that the carbon nanomaterials (CNMs) used for the modification of TiO_2 photoanode were mostly prepared via tedious methods involving more steps and energy consumption.[40] Moreover, it is necessary to understand the structure and role of CNMs in the electron collection and transport at the interface of the photoanode of a DSSC device. The effects of size selected CNMs are rarely investigated. To best of our knowledge, double dialysis method is adopted for the first time for selecting size controlled CNMs (~ 2 nm sized sheets) for DSSC application. In this study, different amounts of CNMs are incorporated in the photoanode to study the PCE of the resultant DSSCs. The loaded CNMs, after heat treatment in air, leave a hierarchical pore structure, which enhances the dye utilization and oxidized dye regeneration as the electrolyte approach to the TiO_2/dye interface is enhanced.

Experimental Section

View Article Online
DOI: 10.1039/D0MA00654H

The details of the materials used are given in the supporting file.

Characterization Techniques

^{1}H NMR (500, 400 MHz) and ^{13}C NMR (125,100 MHz) spectrum of carbonaceous nanomaterials were recorded on a Bruker NMR spectrometer in D_2O with tetramethylsilane as an internal standard. Fourier-transform infrared (FTIR) spectra were recorded with JASCO FTIR–4100 spectrometer using KBr cell and 1064 nm laser. Powder X-ray diffraction (PXRD) was recorded using a Bruker D8 advance diffractometer equipped with Cu Kα source (1.5406 Å). The solution state absorption spectra were measured in a JASCO V-650 UV-visible spectrophotometer. Diffuse reflectance UV-Vis spectra were recorded employing a JASCO model V-570 solid-state UV-Vis spectrometer. Emission spectra were measured in $CHCl_3$ solvent using a JASCO FP-6300 spectrofluorimeter. Photovoltaic performance (current density *vs*. voltage, *J-V*) was measured under one sun condition using LOT technologies solar simulator equipped with 150 W xenon lamp and air mass (AM) 1.5 global filter, which provided a light power of 100 $mWcm^{-2}$. The spectral intensity of the solar simulator is chosen considering the short-circuit current from the standard silicon solar cell (Type: RC2-1010, SN: 0520160006, SPD laboratory, Inc.). A dark mask with a circle-shaped opening in the middle was placed on the DSSC to expose the active area of the DSSC to light. Electrochemical impedance spectroscopy (EIS) measurement was performed using MetrohmAutolab 302N potentiostat/galvanostat(AUT86242) with the FRA32M module controlled by N0VA 1.11 software.EIS fitting was done using ZSimWin 3.6 software.

Synthesis of CNMs

Citric acid, sucrose and dithiobiurea in the weight ratio of 2:2:1 was initially dissolved in 50 mL of ultrapure water by sonication for 20 minutes. Then, the resulted colorless clear solution was transferred into a Teflon lined stainless steel autoclave (100 mL capacity) and kept in a muffle furnace at 180 °C for 8h.[41] After cooling down the autoclave, the unreacted residues were removed by filtration, and the clear orange filtrate was centrifuged at 3000 rpm for 15 minutes to remove the minute suspended particles. Further, the clear supernatant solution was loaded in a separating funnel and washed with dichloromethane to remove the unreacted organic moieties. Finally, it was filtered via a 0.2-micron (pore size of 200 nm) cellulose syringe filter followed by volume reduction through the distillation method.

Size selective separation of CNMs

The clear orange solution from the above step was dialyzed against ultrapure water using a dialysis membrane tube with a molecular weight cut off (MWCO) of 0.5–1 kDa (pore size, 1.5 nm) for 24 h. This process will allow the small organic moieties of the size of less than 1.5 nm (maximum of 15 Å) to exit the dialysis tube. Dialysis bath water was changed in every 6 h to avoid the accumulation/deposition of particles inside the dialysis tube wall.

View Article Online
DOI: 10.1039/D0MA00654H

After 24 h of dialysis, particles of size >1.5 nm were left inside the tube. The product left inside the tube (> 1.5 nm – 200 nm) was subjected to second time dialysis against ultrapure water in a dialysis membrane bag with MWCO of 10-15 kDa (pore size, 3 nm) for another 24 h. The water outside turned pale yellow due to CNMs of size ranging from 1.5 to 3 nm is exiting in the dialysis tube. This pale-yellow solution was collected and evaporated in a vacuum oven to obtain dark brown colored shining particles called CNMs. The various stages of the synthesis of size-selective CNMs are shown in the supporting information (Scheme S1).

CNMs loaded TiO_2 film electrode preparation

The photoanode was prepared by following the reported method, and the typical preparation procedure is as follows. The fluorine-doped tin dioxide coated glass plates (FTO plates) were initially cut down using a diamond cutter in the dimensions of 1.5 cm x 1.75 cm. The plates were left immersed for 15 minutes in a soap solution, ultrapure water (two times), acetone, and isopropyl alcohol while maintaining sonication. The cleaned and dried plates were treated with 40 mM aqueous $TiCl_4$ at 70 °C for 30 minutes. The $TiCl_4$ treatment was repeated for two times, and the plates are washed with double distilled water followed by ethanol. Further, the plates were heated in a muffle furnace at 500 °C for 30 minutes and allowed to cool down to room temperature naturally. $TiCl_4$ treated conducting side of FTO was coated with transparent nano-titania paste loaded with various wt.% of CNMs (5 mg of CNMs was dispersed in 5 ml of methanol and 0.1, 0.25, 0.5, 0.75, 1 and 1.5 ml of methanol dispersion was added to each 100 mg titania paste and stirred for 12 h at the ambient condition) by doctor blade technique using a mask with a circular hole. The thickness of the transparent is around 5-6 µm, and the coated area is 0.196 cm^2. The TiO_2 coated plates were heated at 500 °C for 30 minutes. Upon cooling the plate, the scattering layer of TiO_2 has been applied (Ti-Nanoxide R/SP, Solaronix) by the doctor blade technique followed by heating at 400 °C for 20 minutes.

N719-dye/CNMs loaded TiO_2 photoanode preparation (FTO/TiO_2-CNMs-N719)

FTO/TiO_2 incorporated with different wt.% of CNMs (0, 0.1, 0.25, 0.5, 0.75, 1 and 1.5wt%) were immersed in N719 dye solution for 12 h (0.5 mM in 1:1 (v/v) ratio of acetonitrile and tertiary butanol solvent mixture) to ensure maximum uptake of dye by the TiO_2.

DSSC fabrication with FTO/TiO_2-CNMs-N719 for *J-V* and EIS measurements

FTO/TiO_2-CNMs-N719 photoanode and Pt counter electrode were assembled into a sandwich-type cell with the help of a 60 µm hot-melt gasket frame (MS004610-10).[42] These cells were then filled with electrolyte through a hole left intentionally open at the back of the counter electrode. The liquid electrolyte consists of LiI (0.1 M), I_2 (0.05 M), t-butylpyridine (0.5 M) and 1-butyl–3–methyl imidazolium iodide (0.6 M) in a mixture of valeronitrile (15%) and acetonitrile (85%). The schematic representation of the device fabricated is shown in the scheme S2.

Results and discussion

Citric acid is used as a carbon source for the graphene core, surrounding functional moieties of the CNMs are derived from sucrose and the presence of N and S hetero atom from dithiobiurea to increase the optical and electrochemical performances. Moreover, the precursor materials used for the synthesis of CNMs are easily accessible and economic. The hydrothermal synthesis method adopted is give up CNMs of size less than 3 nm with S and N functional tethered to it. The proposed mechanism for the formation of CNMs is shown in scheme 1. It starts with dehydration followed by various processes, including hydrothermal degradation, polymerization and carbonization leading to nucleation and growth of CNMs. The structure of CNMs is like two or three layers of nanometer sized staked sheets of graphene covered with amorphous shell which bearing various functional moieties.[35,43]

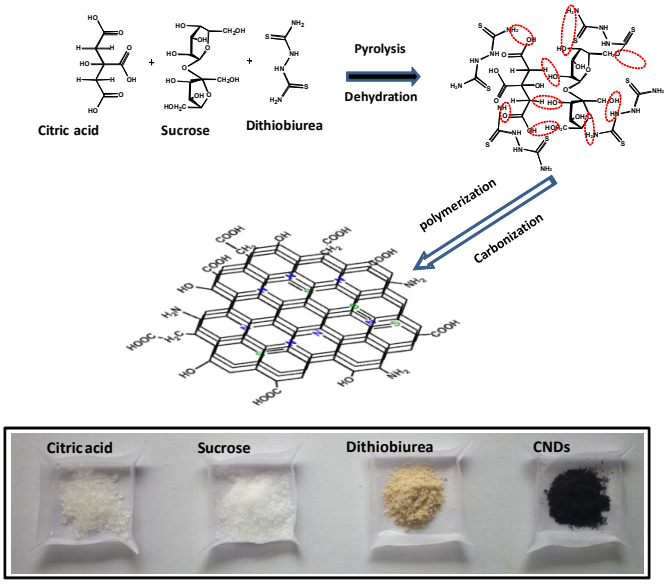

Scheme 1: Proposed mechanism for the synthesis of CNMs

The SEM image (Figure 1a) at 500 nm scale (60000 x magnifications) shows a transparent layered structure of CNMs. The energy dispersive X-ray spectrum (figure S1a) confirms the presence of carbon, oxygen, nitrogen and sulphur. The elements are originated from the precursors, and their atomic percentage is given in figure S1a (insert). HR-SEM is used to understand the surface morphology of the photoanode fabricated with and without CNMs, and the images are shown in figure 2. It is observed that the surface of the film is smooth for TiO_2, and for TiO_2 with 0.5 wt.% loading of CNMs, few holes and surface cracks are there (figure 2a and 2b). This may due to the degassing of the surface functional groups of CNMs while heating the TiO_2 films at 500 °C. EDAX does not detect any N and shows a trace of S (0.8%, Table S1). Therefore, to understand the presence of carbon, CHNOS analysis was performed (Table S2). CHNOS confirms only trace amount of N and S, therefore most of the CNMs incorporated into the photoanode

degassed during the annealing step forming porous TiO_2 film, which probably enhanced the light scattering just like the hierarchical spheres of TiO_2 making second structure which is concentric spherical or three dimensional in shape.[44]

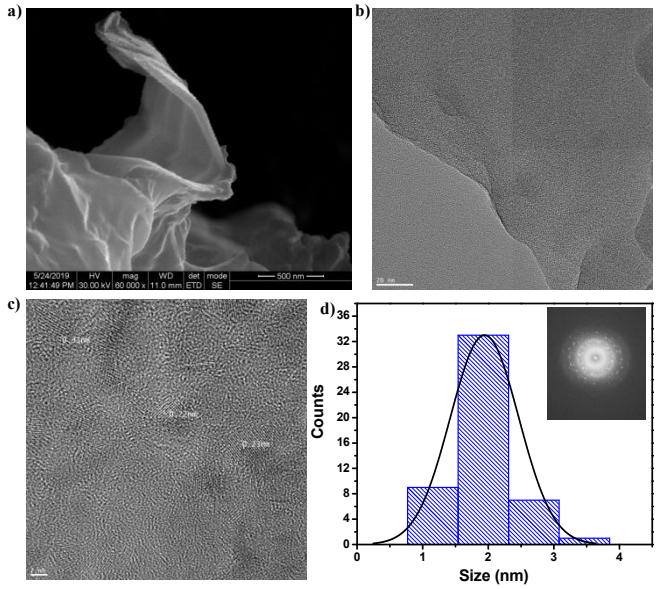

Figure 1: a) HR-SEM image (at 60k magnification), b) HR-TEM image (20 nm scale) of CNMs C) HR-TEM image (2 nm scale) of CNMs and d) particle size histogram (inset FFT image) derived from the image of 1b.

Three-dimensional shape and exact particle size details are derived from HR-TEM measurements shown in figure 1b. The transparent layered structure of CNMs is confirmed through HR-TEM micrographs shown in figure S1b (50 nm scale, 500000 x magnifications). The presence of particles of 1.5 to 3 nm in size is discernible (figure 1b) from the particle size histogram (figure 1d). Presence of lattice fringes with spacing 0.23 nm and 0.31 nm are possibly related to the (100) and (101) planes of CNMs (figure 1c). Further, the Fast Fourier Transform (insert of figure 1d) image shows the crystalline nature of the prepared CNMs. Atomic force microscopic (AFM) measurement gives the surface roughness with topographic details measured via the non-contact mode (figure S1c). It indicated the layered quasi-spherical sheet structure of CNMs. The root mean square roughness value obtained from the AFM measurement is 1.85 nm, indicating the smooth surface of the prepared CNMs.

AFM has also been used to analyze topographic details of the TiO_2 photoanode prepared with and without CNMs (figure S2a and b), and it is observed that the roughness for bare TiO_2 is around 8.3 nm was increased to 14.60 nm while loaded with 0.5 wt.% of CNMs. Profilometry is one of the tool and is useful to understand the surface roughness of a material and thickness of hierarchical porous architecture (thickness of the transparent TiO_2 layer is around 5-6 µm, and the coated area is 0.196 cm^2). It has been done for the bare TiO_2 photoanode as well as for the TiO_2 loaded with 0.5 wt% CNMs. The thickness of the TiO_2 and TiO_2 loaded with 0.5 wt.% CNMs are 9.6 µm and 8.5 µm, respectively. The average roughness of the TiO_2 photoanode in the absence of CNMs is 234.36 nm which has increased in the presence of 0.5wt.% of CNMs to 462.14 nm. From the profilometry images we could see that the bare TiO_2 film has smooth surface (figure S3a) compared to that of the film loaded with CNMs. Moreover, film loaded with CNM exhibits pores (figure S3b) developed by the burning of CNMs during the annealing step. AFM and HR-SEM results also validates the presence of pores as conversed earlier. BET surface area of CNM, TiO_2, and 0.5 wt.% CNM incorporated TiO_2 are 2.31, 64.76, and 53.07 $m^2\ g^{-1}$, respectively. N_2 isotherm and pore size distribution analysis are shown in figure S4a and b. Pore size distribution analysis (Table S3) indicates the widening of pore volume from 0.32 to 0.45 cm^3/g and average pore size from 13.43 to 25.31 nm upon incorporating CNM into TiO_2. Degassing of CNMs, during annealing, could have widened the pores which consequently reduces the surface area as mentioned above.

View Article Online
DOI: 10.1039/D0MA00654H

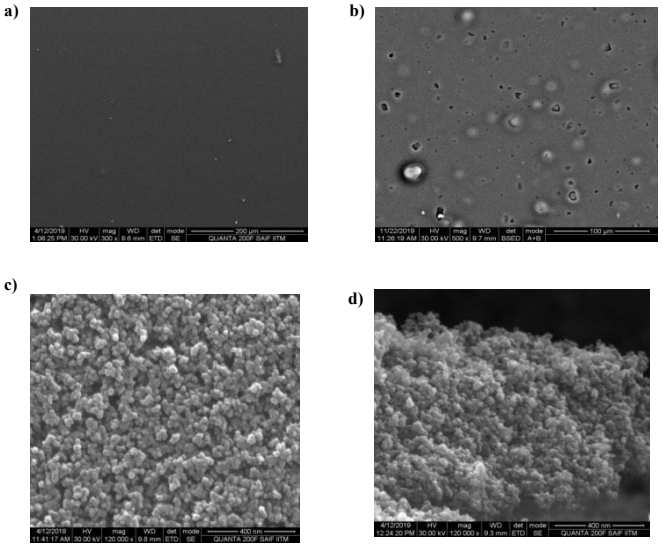

Figure 2: HR-SEM analysis of bare transparent TiO_2 film (a,c) and TiO_2 with 0.5 wt% of CNMs (b,d).

Elemental composition and functional group details of CNMs and CNMs incorporated photoanode

Elemental analysis of CNMs confirms the presence of 40.84% of carbon, 4.72% hydrogen, 10.70% of nitrogen, 9.99 % of sulphur and 36.61% of oxygen (Table S2), which are originated from the precursors used for the synthesis. FT-IR spectroscopy of CNM (figure S5a) elucidates presence of -C-H, -NH, -C–OH, -NH-CO, and -SO_3H stretching vibration at 3035 cm^{-1}, 3129 cm^{-1}, 1166 cm^{-1}, 1404 and 620 cm^{-1} respectively. FT-IR spectrum of TiO_2 indicates peaks at ~ 3406 cm^{-1} due to the –OH stretching vibrations of the surface functional groups. The peaks below 1000 cm^{-1} are due to various modes of vibration of Ti-O-Ti. TiO_2 with 0.5 wt.% CNM shows new peaks at 1660 cm^{-1} correspond to C=C and C=O stretches originating from CNMs. ^1H NMR spectrum (figure S5b) shows signals in both down and upfield area, confirming the presence of both aliphatic and aromatic groups. For instance, the signals in the high shielding area, from 2.75-3.2 ppm, are consistent with the aliphatic protons. The signals in the region of above 6.5-8.2 ppm are for aromatic protons of carbon sheets and carboxylic functional moities. The middle-range signals of 5-6.5 ppm are for the protons

of various functional groups like hydroxyl, amino, epoxy, etc. Besides, the ^{13}C NMR (figure S5c) shows the signal in three regions: 40-50 ppm, which is assigned to sp^3 carbon atoms attached with –OH group, 70-80 ppm, which are associated with the ether linkages and peaks above 180 ppm assigned to carbonyl carbon (-C=O). The results from NMR analysis are concurring with the previous reports from carbonaceous nanomaterials.[45] The thermal stability of the prepared CNMs has been analyzed via a thermogravimetric measurement in the air atmosphere at a temperature ramping rate of 10°C min^{-1} (figure S5d). This weight loss may be due to the degradation of amorphous shell of CNMs. PXRD (figure S6) of CNMs elucidate the amorphous nature of CNMs as a broad peak of (002) plane was seen at 20-24 °.

Photophysical properties

The UV-visible absorption spectrum (figure S7a) of CNMs exhibit two peaks, one at λ_{max}= 280 nm and other at 352 nm, the former is assigned to π–π* electronic transition raised from the C=C bonding and the later one assigned to n–π* transition from the heteroatoms present on the surface. The photoluminescence has been measured to study the electron-hole recombination and surface defects on CNMs surface (figure S7a). In which the CNMs show emission at 540 nm while the excitation is fixed at 360 nm. To check the excitation dependency, the emission is monitored for various excitation wavelengths from 300-480 nm in the interval of 20 nm, which shows that the prepared CNMs is exhibit the excitation dependent emission behaviour (figure S7b), and it is probably due to the presence of various surface trap states and emissive states. Further, the fluorescence decay is monitored at a wavelength of 540 nm (excitation of 365 nm). The emission decay profile of CNMs is fitted with multi-exponential decay (figure S7c) with an average lifetime of 4 ns. This provide evidence for the presence of various emissive states.[45] For better understanding of the emission behaviour of CNMs, excitation and emission contour map of CNMs in 3D view is illustrated in figure S8a and b which indicate the multicolor photoluminescence characteristic of CNMs. The photoexcitation of carbonaceous nanomaterial is is due to π-plasmon absorption from the core carbon nanoparticles.[46] Figure S9 shows the absorption spectra of neat TiO_2 and CNM loaded TiO_2 (0.5 and 1 wt.%) measured in solid state clearly indicating scattering of light by CNMs loaded TiO_2 in the visible region. This increase in scattering is probably due to additional pores generated in the photoanode by CNMs. Therefore, employing CNMs could affect the amount of light available for the dye excitation. The surface coverage of the N719 dye on hierarchical porous architecture is also investigated. Typically, the high surface coverage could be achieved when the surface area of TiO_2 is large. However, we have observed the different trend such as the dye loading was decreased with increase in CNMs (figure S10). This may due to the porous nature of TiO_2 surface by the incorporation of CNMs which may reduce the anchoring of more number of dyes on TiO_2. Thus, hierarchical porous architecture will help to avoid aggregation between the dye molecules on the surface, as a result high PCE is achieved. Thus, the optimization of CNMs is required to enhance the PCE of DSSCs.[47,48]

J-V measurements of DSSC

View Article Online
DOI: 10.1039/D0MA00654H

Photoanodes prepared with 0, 0.1, 0.25, 0.5, 0.75, 1, and 1.5 wt.% of CNMs were assembled into DSSC (Scheme S2) and subjected to J-V measurements, and their performance is compared in figure 3a.

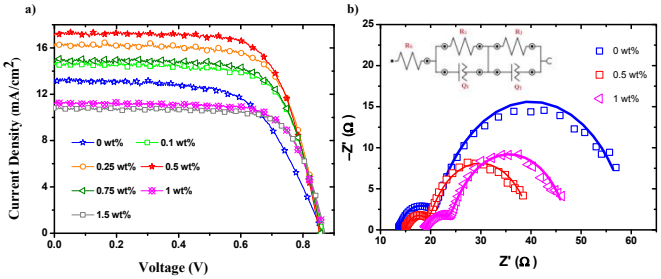

Figure 3: a) *J–V* plots of DSSCs having different wt.% of CNMs in their photoanodes and b) Nyquist plot obtained at 1 sun condition at *Voc* for photoanodes loaded with 0, 0.5 and 1 wt.% of CNMs (Solid lines are the fit to the data).

Table 1 shows the different parameters calculated from the J-V characteristics such as *Jsc*, *Voc*, FF (fill factor), and PCE. Upto a loading of 0.5 wt.%, the PCE has increased and beyond which it decreases, probably due to light absorption inhibited by excessive CNMs in the photoanode. The PCE of photoanode devoid of CNMs is 7.01% and which increases to 10.24% for photoanode loaded with 0.5 wt.% of CNMs (almost 46% of enhancement in PCE upon incorporating the CNMs). The decrease in PCE, as well as *Jsc* with the higher loading of CNMs, may due to over-accumulation of CNMs on the TiO_2 surface promoting the back-electron transfer. There are no apparent variations in the *Voc*, and FF measured for various loadings of CNMs, and PCE has mostly stay on with *Jsc* controlled, which is dependent on the electron injection ability of the dye into the CB of TiO_2 as well as the charge collection efficiency of TiO_2. **Table S4** shows the comparison of literature reports pertains to CNMs based DSSCs. To the best of our knowledge, we do not find any work on incorporating size-controlled CNMs in enhancing PCE.

Table 1: Photovoltaic parameters measured under 1 sun condition from DSSC fabricated with different wt.% loading of CNMs.

CNMs (wt %)	*Jsc* (mA cm^{-2})	*Voc* (V)	FF	η (%)	Avg. η for 3 cells (%)
0	13.10	0.864	0.61	7.01	7.01
0.1	14.56	0.860	0.70	8.84	8.25
0.25	16.23	0.858	0.70	9.85	9.74
0.5	17.18	0.852	0.69	10.24	10.15
0.75	14.94	0.858	0.70	8.90	8.53
1	11.24	0.858	0.72	7.01	6.98
1.5	10.82	0.873	0.72	6.87	6.55

Electrochemical Impedance analysis

The Nyquist plot shows two semicircles. The one at the high-frequency region corresponds to the charge transfer at the counter electrode/electrolyte interface. The second one in the mid-frequency region is due to the photoanode/electrolyte interface. The equivalent circuit chosen to fit the data is shown as an inset to Figure 3b, which is $R_s(R_1Q_1)(R_2Q_2)$. R_s, R_1, and R_2 are solution-cum-contact resistance, charge transfer resistance at counter electrode/electrolyte and photoanode/electrolyte interfaces. Q_1 and Q_2 are the constant phase element associated with the R_1 and R_2, respectively. **Table S5** summarizes all the passive elements estimated through the fitting for CNMs loadings of 0, 0.5 and 1 wt.%. R_s increases with the CNMs loading as it modifies the TiO_2 film consequences the contact resistance with FTO. R_1, charge transfer resistance across counter electrode-electrolyte interface, is 7, 4.8 and 5.2 W for CNMs loading of 0, 0.5 and 1 wt% respectively. Given the large error in the admittance (Y1) associated with the Q1, which is a constant phase element associated with R_1, for the practical purpose, we can assume that R_1, is nearly the same. Whereas, R_2, which is measured across photoanode/electrolyte interface, significantly decreases from 39.0 to 20.5 W, while the CNMs loading is enhanced from 0 to 0.5 wt.% and 23.46 W when the loading is raised to 1 wt.%. Since these values are measured at one sun condition and *Voc* applying 10 mV of sinusoidal AC perturbation, the equilibrium concentration of electron in the CB of TiO_2 is a function of exciton recombination, and back electron transfer to the oxidized dye, making the net current across the photoanode/electrolyte interface zero. The applied alternative current perturbation modulates the current across the photoanode/electrolyte interface, which captures the charge transfer resistance associated with the electron transfer from the photoanode to the I_3^- in the electrolyte and/or electron transfer from the I^- to the oxidized dye in the photoanode. In our study, we find a decrease in R_2 and an increase in PCE at 0.5 wt.% of CNMs compared to the CNMs free photoanode. Therefore, the reduction in R_2 is due to the effective dye regeneration by the I^- in the electrolyte.

As observed from HR-SEM analysis, the size and amount of pores produced due to degassing of CNMs could be optimum at 0.5 wt.% of CNMs loading, making it easier for the electrolyte to access the oxidized dyes present in the pores of the TiO_2 layer. The pores produced by the CNMs are bigger than the inherent pore size of the TiO_2 film; therefore, including of CNMs is concluded to create a hierarchical pore structure improving the DSSCs performance.

Conclusions

CNMs in size range 1.5 to 3.5 nm were incorporated with the mesoporous TiO_2 semiconductor in the photoanode of DSSC. To best of our knowledge, this is the first report on using size selected CNMs into the photoanode of the DSSC. Based on SEM analysis formation of wide pores and cracks in the photoanode upon incorporating CNMs is understood. These pores may be assisting in the free flow of electrolyte into the photoanode, reducing the over potential related to the oxidized dye regeneration. This could be the reason behind the improved *J*sc observed. For the optimized 0.5 wt.% CNMs loaded photoanode, *J*sc increased from 13.10 mA cm^{-2} to 17.18 mA cm^{-2}.

Conflicts of interest

There are no conflicts to declare.

Acknowledgements

M.A.J. acknowledges SERB for the TARE project (Ref: TAR/2018/00048, Dt: 18.02.2019). M.A.J. also acknowledges SAIF and department of Chemistry, IIT Madras for analytical measurements. V.S. thanks to the Department of Chemistry and BSACIST for the Senior Research Fellowship. S. J thanks for fellowship received through SERB-N-PDF (PDF/2016/002201) and DST/TMD/SERI/HUB/1(c). Authors acknowledge the funding through DST/TMD/SERI/HUB/1(C) for establishing DSEHC (DST-IITM solar energy harnessing center). M.A.J acknowledges Mr. Ganapathirao Kandregula, research student of Prof. KR group for the assistance in impedance fitting. M.A. J also acknowledges to department of Metallurgical and Materials Engineering for Titan 80-300 TEM facility.

References

1 N. Kannan and D. Vakeesan, *Renewable and Sustainable Energy Rev.,*2016, **62**, 1092.

2 K. Fan, J. Yu and W. Ho, *Mater. Horiz*., 2017, **4**, 319-344.

3 Q. Zheng, H. Kang, J. Yun, J.Lee, J. H. Park and S. Baik, *ACS Nano,*2011, **5**, 5088–5093.

4 C. -J. Lin, W. -Y. Yu and S.-H.Chien, *J. Mater. Chem.,* 2010, **20**, 1073–1077.

5 Y. J. Kim, M. H. Lee, H. J. Kim, G. Lim, Y. S. Choi, N. -G. Park, K. Kim andW. Lee, *Adv. Mater.,* 2009, **21**, 3668–3673.

6 Y. -C. Park, Y.- J. Chang, B.-G. Kum, E.-H. Kong, J. Y. Son, Y. S. Kwon, T. Park and H. M. Jang, *J. Mater. Chem.,* 2011**,*21***, 9582–9586.

7 J. Lin, Y. -U. Heo, A. Nattestad, Y. Yamauchi, S. X. Dou and J. H. Kim, *Electrochim. Acta,*2015, **153**, 393–398.

8 Y. Li, H. Wang, Q. Feng, G. Zhou and Z. -S. Wang, *Energy Environ. Sci.,* 2013, **6**, 2156–2165.

9 X. Dang, J. Qi, M. T. Klug, P. Y. Chen, D. S. Yun, N. X. Fang, P. T. Hammond andA. M. Belcher, *Nano Lett.,*2013, **13**,637–642.

10 H. Choi, W. T. Chen andP. V. Kamat, *ACS Nano,*2012, **6**,4418–4427.

11 N. Yang, J. Zhai, D. Wang, Y. Chen and L. Jiang, L. *ACS Nano,*2010, **4**, 887–894.

12 L. Chen, Y. Zhou, W. Tu, Z. Li, C. Bao, H. Dai, T. Yu, J. Liuand and Z. Zou, *Nanoscale,*2013, **5**, 3481–3485.

13 T. Ma, M. Akiyama, E. Abe and I. Imai, *Nano Lett.,*2005, **5**, 2543–2547.

14 K. Mahmood and S. B. Park, *J. Mater. Chem. A,*2013, **1**,4826–4835.

15 H. Tao, W. Chen, J. Wang, W. Ke, J. Wan, J. Wu and G. Fang, *Electrochim. Acta,*2014, **137**, 17–25.

16 A. K. Chandiran, M. K.Nazeeruddin and M. Gra¨tzel, *Adv.Funct. Mater.*, 2014, **24**, 1615–1623.

17 H. Elbohy, A. Thapa, P. Poudel, N.Adhikary, S. Venkatesan and Q. Qiao,*Nano Energy,* 2015, **13***,* 368–375.

18 S.-W. Lee, K.-S. Ahn, K. Zhu, N. R. Neale andA. J. Frank, *J. Phys. Chem. C,*2012, **116**, 21285–21290.

19 A. Lamberti, A. Sacco, S. Bianco, D. Manfredi, F. Cappelluti, S. Hernandez, M. Quaglio andC. Pirri,*Phys. Chem. Chem.Phys*., 2013, **15**, 2596–2602.

20 Y. Li, Z. Liu, C. Liu, J. Ya, W. Zhao, Q. Chen and J. Bai, *J. Am. Ceram. Soc*., 2012, **95**, 1343-1347.

21 Z. Liu, Y. Li, C. Liu, J. Ya, W. Zhao, D. Zhao and L. An, *ACS Appl. Mater. Interfaces*, 2011, **3**, 1721-1725.

22 Z. Liu, Y. Li, C. Liu, J. Ya, W. Zhao, E. Lei, D. Zhao, and L. An, Solid State Sci., 2011, **13,** 1354-1359.

23 L.-L. Li, C.-Y. Tsai, H.-P. Wu, C.-C. Chen, E. W.-G. Diau,*J. Mater. Chem.,*2010, **20***,* 2753–2758.

24 W. -Q. Wu, Y. -F. Xu, C. -Y. Su andD. -B. Kuang, *Energy Environ. Sci.,*2014, **7**, 644–649.

25 F. Sauvage, D. Chen, P. Comte, F. Huang, L. -P. Heiniger, Y.-B.Cheng, R. A.Caruso andM. Graetzel, *ACS Nano,*2010, **4**, 4420–4425.

26 X. Tao, P. Ruan, X. Zhang, H. Sun andX. Zhou, *Nanoscale,*2015, **7**, 3539–3547.

27 X. Li, J. Yu and M. Jaroniec, *Chem. Soc. Rev.,*2016, **45**,2603–2636.

28 H.-Y.Chen,D.-B.Kuang andC.-Y.Su,*J. Mater. Chem.,*2012, **22**, 15475–15489.

29 Q. Zhang and G. Cao,*J. Mater. Chem.,* 2011, **21**, 6769–6774.

30 S. D.Standridge, G. C. Schatz andJ. T. Hupp,*J. Am. Chem. Soc.,*2009, **131**, 8407–8409.

31 V. D. Dao, P.Kim, S.Baek, L. L.Larina, K.Yong,R.Ryoo, S. H.Ko and H. S. Choi,*Carbon,*2016, **96**, 139-144.

32 S. Kushwaha, S. Mandal, S. Subramanian,S. Aryasomayajul and K. Ramanujam, *Chemistry Select,*2016, **1**, 6179–6187.

33 S. Paulo, E. Palomaresand andE.M. Ferrero, *Nanomaterials,*2016, **6***,* 157-176.

34 S. Thulasi, A. Kathiravan andM. Asha Jhonsi, *ACS Omega,*2020, **5**, 7025−7031.

35 W. Youfu andH.Aiguo, *J. Mater. Chem. C*, 2014, **2**, 6921-6939.

36 Z. Xiang, X. Zhou, G. Wan, G. Zhang and D. Cao, *ACS Sustainable Chem. Eng.,*2014, **5**, 1234-1240.

37 N. Yand, J. Zhai, D. Wang, Y. Chen andL. Jiang,*ACS Nano,*2010,**4**, 887-894.

38 G. Cheng, M. S. Akhtar, O. B. Yang, F. J. Stadler, *ACS Appl. Mater. Interfaces,*2013,**5(14)**, 6635-6642.

39 L. Chen, Y. Zhou, W. Tu, Z. Li, C. Bao, H. Dai, T. Yu, J. Liuac andZ. Zou, *Nanoscale,*2013, **5**, 3481.

40 X. Yan, X. Cui, B. Li andL. S. Li, *Nano Lett.,*2010, **10**, 1869–1873.

41 S. Paulo, E. Palomares and E. M. Ferrero, *Nanomaterials,*2016, **6(9)**, 157.

42 X. ang, T. Ma, G. Guan, M. Akiyama, T. Kida andE. Abe, *J.Electroanal. Chem.,*2004, **570**, 257–263.

43 S. Dong, X.Yuqing, Z.Weimin, Z.Hongtao, Z. Ying, Q.Xiting, M. Yanfeng, Y. Yong andC. Yongsheng, *J. Power Sources*, 2018, **384**, 328-333.

44 J.-Y.Liao, J.-W.He, H.Xu, D.-B.Kuang andC.-Y. Su, *J. Mater. Chem.,*2012, **22**, 7910–7918.

45 V. Srinivasan, M. Asha Jhonsi, M. Kathiresan, A. Kathiravan,*ACS Omega* 2018, **3**, 9096−9104.

46 X. Fang, M. Li, K. Guo, J. Li, M. P. Li hua, B. M.Luoshan and X.Z. Zhao, *Electrochim. Acta,*2014, **137**, 634-638.

47 L. Chen, Y. Zhou, W. Tu, Z. Li, C. Bao, H. Dai, T. Yu, J. Liuac and Z. Zou, *Nanoscale,* 2013, **5**, 3481-3485.

48 K.A.S. Fernando, S. Sahu, Y. Liu, W. K. Lewis, E. A. Guliants, A. Jafariyan, P. Wang, C. E. Bunker and Y.-P. Sun, ACS Appl. Mater. Interfaces, 2015, **7**, 8363–8376.